Multicentury climate warming slows meridional overturning circulation, sequestering nutrients in the deep ocean and reducing uptake of anthropogenic CO_2

Y. Liu[1], J.K. Moore[1], and F. Primeau[1]

1 - University of California, Irvine, Irvine, CA, USA.
Corresponding author: Yi Liu (yil45@uci.edu)

Key Points:

- Global meridional overturning circulation will drastically decrease to the year 2300 under high-end emission scenarios.
- Deep circulation slowdown drives long-term sequestration of nutrients and dissolved inorganic carbon in the deep ocean.
- Ocean dissolved oxygen concentrations steadily decline, with the potential for anoxia eventually developing in some regions.

Abstract

Under a high-end emission scenario to the year 2300, climate warming drives a drastic slowdown in the ocean's meridional overturning circulation, with a cessation of Antarctic Bottom Water (AABW) production and North Atlantic Deep Water (NADW) formation reduced to 5 Sv. In conjunction with regionally enhanced biological production and upper-ocean nutrient trapping in the Southern Ocean, this deep circulation slowdown drives long-term sequestration of nutrients and dissolved inorganic carbon in the deep ocean, but also greatly reduces the ocean's capacity to take up heat and anthropogenic CO_2 from the atmosphere, prolonging peak warmth climate conditions. Surface nutrients (N, P, and Si) are steadily depleted driving down biological productivity and weakening the biological pump, which transfers carbon to the ocean interior. Ocean dissolved oxygen concentrations steadily decline, with the potential for anoxia eventually developing in some regions. This Community Earth System Model (CESM) simulation did not include active ice sheet dynamics, but the strong climate warming simulated would lead to large freshwater discharge from the Antarctic and Greenland ice sheets. This would further stratify the polar regions, potentially leading to complete shutdown of the meridional overturning circulation. The impacts of this would be catastrophic as the hothouse Earth climate conditions could be extended for thousands of years, with widespread ocean anoxia developing, driving a mass extinction event.

Key words: Climate change, nutrient distributions, Southern Ocean

1 Introduction

In the oceans, nutrients and light availability are essential for phytoplankton to subsist and together with temperature control the biological productivity, which directly affects food supply for higher trophic levels. Surface nutrients also affect the efficiency of biological pump, which exports some of the organic matter produced to the ocean interior, decreasing surface water DIC concentrations, affecting air-sea CO_2 flux, atmospheric CO_2 and climate. Sinking organic particles decompose releasing nutrients, consuming dissolved oxygen (DO) and decreasing DO levels in the ocean interior. Ultimately, these exported nutrients and carbon are returned to the surface through the large-scale meridional overturning circulation.

Global nutrient distributions are shaped by both biological and physical processes in the Southern Ocean. Upwelling at the Antarctic Divergence is the main route for nutrients to return to the upper ocean (Sarmiento et al., 2004; Marinov et al., 2006; Primeau et al, 2013). Strong light and iron limitation of phytoplankton growth greatly reduces the utilization of the upwelled nitrate, phosphate, and silicic acid, allowing most of it to move northward in the surface Ekman layer. These waters eventually subduct with the formation of Antarctic Intermediate Water (AAIW) and Subantarctic Mode Water (SAMW) that carries the nutrients into the low latitude thermocline, ultimately fueling low-latitude biological production (Marinov et al., 2006). Primeau et al (2013) imposed increased levels of biological production in the Southern Ocean and showed that increasing the efficiency of the biological pump in the high latitude Southern Ocean directly led to decreasing global productivity, as the reduction in the northern Ekman transport of nutrients out of the Southern Ocean suppressed biological production across the low latitudes. A number of studies have illustrated this inverse relationship between global productivity and production in the high latitude Southern Ocean (Sarmiento et al., 2004; Dutkiewicz et al., 2005; Marinov et al., 2006; 2008; Bronselaer et al., 2016) by artificially modifying forcings or levels of productivity in the Southern Ocean.

Previous studies have examined the response of marine ecosystems to climate change under different warming scenarios to the year 2100. Steinacher et al (2010) used four coupled carbon cycle-climate models to project net primary production (NPP) and export production (EP) over the 21st century and found both of them decreased between 2% to 20% at the global scale. Moore et al (2013) found surface ocean nutrients and biological productivity decreased globally under both the RCP4.5 and RCP8.5 scenarios based on simulation with Community Earth System Model version1 (CESMv1.0). Fu et al (2016) investigated climate change impacts on net primary production and export production with nine Earth systems models (ESMs) in the framework of fifth phase of the Coupled Model Intercomparison Project (CMIP5). Almost all CMIP5 models agreed with global-scale increases in stratification, which are accompanied by decreases in surface nutrients, NPP and EP. Bopp et al (2013) found Southern Ocean NPP increased to the year 2100 which showed opposite trends as global oceans because of the alleviation of light limitation and/or temperature limitation. Leung et al (2015) also found increased NPP in the Antarctic band (south of ~65^{o}S) to the end of 21st century across the CMIP5 Earth System Model suite.

Deoxygenation is considered one of the key stressors of ocean ecosystems under climate change in the 21st century. Bopp et al (2013) analyzed 10 ESMs in the framework of CMIP5 for each of the IPCC's representative concentration pathway (RCPs) and found that deoxygenation operated globally with the largest DO decreases in ocean intermediate and mode

waters. Stramma et al (2008) found evidence for expansion of the oxygen-minimum zones (OMZs) in the tropical oceans in the current era. The deoxygenation reflected the combined effects of both physical and biological processes, such as reduced oxygen solubility from warming, reduced ventilation from stronger stratification, circulation changes (Keeling et al., 2010), and shifts in the magnitude of organic matter decomposition, which is controlled by nutrient distributions and export productivity (Hofmann and Schellnhuber, 2009).

Many researchers also worked on air-sea CO_2 exchange and anthropogenic carbon storage to the end of 21st century, and they agreed with the increase of pCO_2 in the surface ocean and anthropogenic carbon storage emphasizing the importance of Southern Ocean uptake (Long et al., 2013; Frölicher et al., 2015; Völker et al., 2015; Hauck et al., 2015; Ito et al., 2015). Friedlingstein et al (2014) quantified the increase of global annual air to ocean carbon flux from nearly zero to stabilize at 6PgC/yr at the end of 21st century which is mainly due to increased anthropogenic CO_2. However, there are still huge model uncertainties in ocean carbon storage between different climate models to the end of 21st century.

These studies provided important insights on climate system impacts on marine ecosystems and the carbon cycle feedbacks onto climate, but in terms of the cumulative effects of climate warming and design of future mitigation policy, climate change projections and climate-carbon feedbacks on longer time scales become critically important. The global temperature is projected to increase to the year 2300 even under low emissions scenario RCP2.6-ECP2.6 (van Vuuren et al., 2011), although the change in magnitude is smaller than high-end emission scenario (Caesar et al., 2013). Randerson et al (2015) extended the CESMv1 climate projections to the year 2300 and found that ocean contributions to the climate-carbon feedback increased considerably and gradually exceeded land contributions after the year 2100, under the high-end RCP8.5-ECP8.5 emissions scenario (van Vuuren et al., 2011). NADW production declined drastically from ~30 Sv in 1990s to 5 Sv in 2300, with about half of the decline prior to year 2100. Most of the ocean heat uptake (85%) and more than half of the anthropogenic CO_2 uptake occurred after year 2100. We previously examined ocean dynamics and biogeochemistry in this same CESM1 simulation to year 2300 (Moore et al., 2018, hereafter MET2018).

MET2018 documented large increases in NPP and EP in the high latitude Southern Ocean driven by natural climate forcings (warming surface waters, declining sea ice cover, shifting winds), which stripped out a higher percentage of the nutrients upwelling at the Antarctic Divergence, reducing the northward flow of nutrients in the surface Ekman layer. The increased export production sinking into the upwelling waters drove a subsurface nutrient buildup (~100 – 1000m, "nutrient trapping"). Subsurface concentrations of nitrate, phosphate, and silicate in this trapping region were still rising at the end of the simulation in year 2300. The Antarctic Divergence upwelling increased in strength by about 25% due to an intensification and southward shift in the mid-latitude westerly winds (MET2018). The nutrient trapping in the Southern Ocean in conjunction with the collapse of deep mixing in the high latitude North Atlantic and the increasing stratification globally as surface temperatures warm, drove a net transfer of macronutrients from the upper ocean (~0-1500m) to the deep ocean (> 2000m). Upper ocean nutrient concentrations declined everywhere outside of the Southern Ocean leading to steady declines in biological production and export production to the ocean interior by the biological pump.

By 2300 global-scale NPP had decreased by 15% and the export carbon flux at 100m had declined by 30%. The increasing nutrient stress in surface waters shifted phytoplankton community composition, with the diatom share of NPP dropping 36% by 2300 (MET2018). Diatoms lead to more efficient export of organic matter in the model, so this community shift accounts for much of the difference in decline between NPP and EP. As the small phytoplankton increasingly dominate, export efficiency is decreased, and the regeneration of nutrients within the euphotic zone increases, boosting NPP with recycled nutrients (Moore et al., 2013; Fu et al., 2016; MET2018). The larger decline in EP may be more indicative of the decline in food resources for higher trophic levels (Fu et al., 2016). Both NPP and EP steadily decline over time everywhere outside of the Southern Ocean, and are still falling at the end of the simulation. Fu et al (2018) found dissolved oxygen (DO) in the oceans declined steadily at the global-scale, but in the low latitude, mid-depth waters associated with the oxygen minimum zones (OMZs) DO declined initially but then partially recovered, beginning to increase around 2150. This oxygen increase was driven by the weakening biological pump, which reduced the subsurface oxygen demand for remineralization.

Here, we present additional analysis of this same CESM V1 coupled carbon-climate simulation to the year 2300. We quantify influences of AABW formation and the deep overturning circulation with strong, persistent climate warming, on the global distributions of key biogeochemical tracers, including nutrients, dissolved inorganic carbon (DIC), and dissolved oxygen (DO).

2 Methods

We conducted a coupled climate simulation with Community Earth System Model CESM1.0(BGC) for the period from 1850 to 2300 under high-end warming scenario RCP8.5-ECP8.5 with prescribed atmospheric CO_2 rising from approximately 285 ppm in 1850 to 1962 ppm in 2250. The CESM1.0(BGC) component simulates multiple plankton functional groups, the key growth limiting nutrients, and fairly complete marine carbon cycle and oxygen cycle representations designed based on Moore et al (2004). The ocean module is the CCSM4 ocean component (Danabasoglu et al., 2012; Gent et al., 2011). Details on model configuration and set up were given by Lindsey et al., (2014). The first part of this simulation (to year 2100) was used in CMIP5 analyses following the RCP8.5 future scenario. This is a business as usual scenario prescribed atmospheric CO_2 values reaching 1962 ppm before leveling the last 50 years of simulation. Global mean surface air temperatures increased 9.6 ^{o}C by year 2300 (Randerson et al., 2015). Evaluation of the marine ecosystem dynamics and the climate change impacts to year 2100 are discussed by Moore et al. (2013). Uptake and storage of anthropogenic CO_2 in the oceans was addressed by Long et al. (2013). Additional documentation and source code are available online (www2.cesm.ucar.edu) and the model output files from this simulation are available through the Earth System Grid Federation (ESGF) data delivery system at (https://www.earthsystemgrid.org/dataset/ucar.cgd.ccsm4.randerson2015.html). We also obtained output from similar RCP8.5-ECP8.5 simulations to 2300 with the MPI-ESM-LR and HadGEM2 ESMs from the ESGF.

We divide the global ocean into smaller units both regionally and vertically for this analysis. To better understand the regional nutrient trapping and sequestration in the deep ocean,

we focus on the high latitude Southern Ocean (90°S-60°S). Vertically the ocean is divided into surface layer (0-100m), subsurface layer (100-1000m), intermediate layer (1000-2000m) and deep waters (>2000m). When studying the impacts of overturning circulation and climate change on ocean tracers, it is often useful to divide the tracers into their regenerated and preformed components. Regenerated nutrients are supplied to the ocean interior by the biological pump as organic matter remineralizes releasing inorganic nutrients and carbon. Preformed nutrients are nutrients unutilized by the phytoplankton that are brought to the ocean interior within subducting water masses.

In the general case, nutrient concentration of a water parcel in the ocean interior consists of two components: the preformed part and the regenerated part. The preformed concentration, $P_{preformed}$, is defined as the nutrient concentration in a water parcel when it was last in the surface ocean before being subducted into the interior. The regenerated concentration, $P_{regenerated}$, is the additional concentration that results from the integrated remineralization of organic matter along the water parcel's trajectory in the ocean interior, i.e.

$$P = P_{preformed} + P_{regenerated}$$

We calculate $P_{regenerated}$ using the apparent oxygen utilization (AOU), which is often defined as $AOU = -\Delta\,[O_2]_{remin}$ and can be obtained directly from the saved model outputs. Take phosphate for example, regenerated nutrient is calculated as follows.

$$P_{regenerated} = r_{P:O_2} \cdot AOU$$

$$P_{preformed} = P - P_{regenerated}$$

Where $P:O_2$ is 1/138. We use similar method to separate regenerated DIC and preformed DIC, which also includes pre-industrial natural ocean DIC concentration.

$$DIC_{regenerated} = r_{C:O_2} \cdot AOU$$

$$DIC_{preformed} = DIC - DIC_{regenerated}$$

Where $C:O_2$ is 117/138. In practice, the model keeps track of remineralization rates and the actual oxygen utilization rate, which are used to distinguish between the preformed and regenerated components.

3 Results

3.1 Slowdown of the Thermohaline Circulation

Both Southern Ocean Meridional Overturning Circulation (SOMOC) and Atlantic Meridional Overturning Circulation (AMOC) gradually slowed down in a warming climate. Global zonal-mean MOC stream function and the corresponding meridional velocities at 50°S and 40°S for key decades (i.e. 1850s, 1990s, 2090s, 2190s and 2290s) showed a weakening trend over time. Vigorous overturning in the upper and lower cells were readily apparent in the 1850s and 1990s, driven by the formation of AABW and NADW, respectively (Figure 1). Both cells weakened and the upper cell shoals by the 2090s, with only remnants of the global overturning circulation remaining in the 2190s and 2290s (Figure 1). The transport of AMOC steadily declined after the year 2000 from 30 Sv in the preindustrial era to stabilize at ~5 Sv after year 2200 (Randerson et al., 2015).

The CESM AABW northward transport at 60°S was 7.7 Sv in the 1990s, which compares well with an estimated rate of 8.1 Sv from CFC observations (Orsi et al., 2002). There was strong northward flow in bottom waters across 50°S and 40°S early in the simulation,

as AABW and entrained waters flowed northwards (inset right panels, Figure 1). This northward flow weakens considerably by the 2090s, and becomes negligible (even reversing direction) later in the simulation, indicating a shutdown of the formation and export of AABW from the Southern Ocean (Figure 1). We find qualitatively similar patterns in two other available ESM simulations to 2300 following the RCP8.5-ECP8.5 scenario, with northward transport in bottom waters early in the simulation and a shutdown in this northward flow by 2300 (Figure S1).

The formation of AABW and NADW drives the overturning circulation. The reduction in NADW formation in the model is driven by the surface warming and increasing stratification in the high latitude North Atlantic with climate change, leading to great reductions in the deep winter mixing seen today across this region (Moore et al., 2013). This deep mixing leads to the formation of NADW and is critical for the biology by entraining nutrients into surface waters. The collapse of deep winter mixing has strong impacts on the biological productivity, with North Atlantic NPP and EP declining nearly 60% by year 2300 (Moore et al., 2013; MET2018).

AABW formation slows due to increasing stratification in the Weddell Sea and the Ross Sea, the key formation regions for AABW in this model, which leads to the slowdown of the Southern Ocean Meridional Overturning Circulation (SOMOC). Stratification in the Weddell Sea (< 60 ^{o}S) increases rapidly beginning just before year 2100 before leveling out near end of the simulation after increasing by more than a factor of 2 (Figure 2). The increase is more gradual in the Ross Sea and begins earlier, though the increase in both regions accelerates with increasing loss of the southern sea ice cover. The increase in both regions is largely driven by reductions in surface salinity (Figure S2). The southern Weddell and Ross seas do not warm as much with climate change (1-2 ^{o}C) as the offshore waters of the Southern Ocean (~6-9 ^{o}C, see Figure 1 MET2018). These regions are kept cooler by the cold winds blowing off Antarctica, and are the only place in the Southern Ocean where some sea ice still forms in the winter months (MET2018).

The slowdown and apparent shutoff of dense AABW formation is apparent in the oxygen fields averaged over the model shelf depths (200-400m, Figure 2). Early in the simulation high oxygen concentrations are seen in the southern Weddell and Ross seas, indicating waters recently in contact with the atmosphere. Over time the increasing stratification breaks this connection to surface waters, and oxygen concentrations then approached values seen offshore, first in the Weddell Sea by the 2090s, within only a small patch of high O_2 water in the Ross Sea by the 2190s (Figure 2). By the 2290s oxygen concentrations declined dramatically across the Southern Ocean at this depth as increasing temperatures decrease solubility at the surface and increasing stratification ensures that winter mixing does not reach this layer. The temperature in this layer increases rapidly after year 2000, with a similar, but weaker, increasing trend seen in the deep SO waters (> 4400m at 60 ^{o}S) (Figure S3). We can track the spread of AABW along the seafloor based on its neutral density (γn>28.27) (Figure S4). The area of AABW in the global bottom ocean gradually decreases in a warming climate, which also provides evidence for the slowdown of thermohaline circulation. The largest decreases in bottom water neutral density are along the deep flow paths out of the Southern Ocean (Figure S4). These patterns reflect the slow down and eventual cessation of northward flowing AABW (Figures 1-2, S1-4).

3.2 Impacts of the Southern Ocean Meridional Overturning Circulation Slowdown on Marine Biogeochemistry

The slowing of the overturning circulation greatly influences the global distribution of the major nutrients, DIC and dissolved oxygen. It contributes strongly to the net transfer of nutrients to the deep ocean documented in MET2018. Surface phosphate in the Southern Ocean gradually decreased over the simulation (Figure 3a) due to the increased biological productivity and export, which overcomes increases in the upwelling flux of phosphate at the Antarctic Divergence (MET2018). In the equatorial region (10°S-10°N), surface PO_4 also gradually decreased, synchronized with the decreases in the Southern Ocean, illustrating the controlling influence of Southern Ocean nutrient dynamics on the lower latitudes. The surface northward transport of phosphate across 50°S and POC flux in the equatorial region both declined steadily over the simulation (Figure 3b). The equatorial upwelling rate declined only slightly over time (~3%, MET2018), so the equatorial productivity declines were driven by the declining subsurface nutrient concentrations. Pasquier and Holzer (2016) also proved that most of the regenerated and preformed phosphorus in low latitudes are from the Southern Ocean northward transport.

The declining northward flux of nutrients in the Southern Ocean surface waters is due to the nutrient trapping around Antarctica, beneath the upwelling zone. Nutrient trapping in the subsurface layer (~100-1000m) started about year 2000 and the concentrations of phosphate, nitrate, and silicic acid rose in a linear fashion all the way to 2300 (Figure 3c). The declines in sea ice cover (Figure 3c) played a key role in boosting Southern Ocean biological productivity (Figure 3e, MET2018). We can compute the contribution of the rising export production to the rising nutrient concentrations, and compare this with the sum effects due to physical processes (by difference from the observed change in concentration) (Figure 3d). Phosphate concentrations in the trapping zone steadily rose due to the increasing biological export, while the sum of physical processes acted to remove nutrients from the trapping zone (Figure 3d) mainly through isopycnal mixing along the upward sloping isopycnals associated with the upwelling zone, but also through the formation of AABW. Both processes transfer some of the trapped nutrients back to the deep ocean.

The declining sea ice cover and the long-term shoaling of Southern Ocean mixed layer depths reduced the light limitation of phytoplankton growth, as seen in the light limitation factors plotted in Figure 3f (see also MET2018). The iron limitation factor on growth does not change much over the simulation, in spite a large increase in the upwelling of dissolved iron (Figure 3f). As iron is the limiting nutrient in this region, the biological productivity will always pull surface concentrations down to similar, low levels. Warming temperatures also acted to increase phytoplankton growth rates (Figure 3f) helping fuel the increases in export production (Figure 3e). Export production continued to increase rapidly after year 2200 when the sea ice cover is nearly gone (Figure 3), driven by the southward shift in the westerlies that eventually pushes the upwelling zone into Antarctica in many regions, leading to coastal upwelling and enhanced iron flux to the surface (MET2018).

To better understand the underlying mechanisms of sequestration of nutrients in the deep ocean, we divided the trends in deep ocean phosphate into the regenerated and preformed fractions (Figure 4b). Phosphate gradually accumulated in the deep ocean after the year 2000,

which can be explained by the increasing regenerated P fraction, as the preformed part decreased slightly. Regenerated phosphate is controlled both by the strength of the biological pump and remineralization rates, and by the transit time through the deep ocean. Globally, export production declined by ~30% over the simulation, so the biological source of phosphate to the deep ocean weakened. Thus, the increasing regenerated phosphate concentrations in the deep ocean must be due to the slowing overturning circulation, which allowed more time for the weakened biological flux to accumulate. We can also break the deep ocean trends in phosphate into the physical and biological drivers (Figure 5). In the Southern Ocean, the increasing export production acted to increase deep phosphate concentrations, while the physical processes acted to remove phosphate (Figure 5a). The physical removal weakens overtime though, contributing to rising deep concentrations, partially driven by isopycnal mixing bringing nutrients down from the trapping zone. Outside the Southern Ocean and at the global scale, the biological contribution to deep ocean phosphate declines as the biological pump weakens (Figure 5b-5c), but this is more than compensated for by the slowing of the overturning circulation, allowing deep ocean concentrations to rise. A similar pattern was seen in the trends for regenerated and total DIC in the deep ocean, but the preformed DIC also increases modestly (Figure 4d). The increase in regenerated DIC is driven by the same processes as for phosphate, while the preformed DIC increases modestly because a fraction of the anthropogenic carbon being taken up by the oceans is being transported to the deep ocean.

Dissolved oxygen concentrations declined over all depth levels within the Southern Ocean (Figure 4a) and at the global scale (Figure 4c). Although there was a modest recovery in the low-latitude, subsurface layer (100-1000m) after year 2150 (Fu et al., 2018). The declines are more rapid in the Southern Ocean (< 60 ^{o}S) particularly in the subsurface nutrient trapping zone (Figure 4a). A simple linear extrapolation of this oxygen decline rate suggests these waters could go anoxic by year 3000. Oxygen declines in the surface layer are driven by decreasing solubility as surface waters warm. At depth the increasing stratification and slowing circulation both contribute to declining O_2. The decreasing oxygen concentrations mirror the rising phosphate concentrations, both driven by the increasing remineralization in the deep ocean.

Global ocean dissolved inorganic carbon concentrations gradually increased over time as the oceans take up more and more anthropogenic CO_2 (Giorgetta et al., 2013), especially in the Southern Ocean (e.g. Ito et al., 2015). Ocean uptake of CO_2 peaked at ~5.5 PgC/yr in the late 21st century and then declined steadily over time, even as atmospheric CO_2 continue to rise, as surface waters become increasingly saturated (Randerson et al., 2015; MET2018). DIC increases in the surface ocean are much larger than in the deep ocean, due to direct uptake of anthropogenic CO_2 from the atmosphere (Figure 6). By the 2190s high concentrations of anthropogenic CO_2 have accumulated throughout the upper ocean down to the depth of the AAIW at ~1500m (Figure 6). In the deep ocean the buildup of DIC over time is due mainly to accumulation of natural carbon via the biological pump and remineralization (~70% of deep ocean DIC increase). The increase in preformed DIC, which include both natural and anthropogenic carbon, accounts for ~30% of the deep ocean DIC increase (Figure 4d).

4 Discussion

One caveat with this study is that the model (like nearly all current ESMs) is not ideally configured to simulate the formation of AABW. The coarse resolution of the ocean model (~1 degree resolution) and the lack of active ice sheets and ocean-ice sheet interactions means the model cannot capture some key smaller scale processes thought to be important in AABW formation. However, the model does form dense waters in qualitatively the correct places (coastal Weddell and Ross Seas) and the northward flow of AABW along the sea floor seems realistic early in the simulation. Historically ESM development has focused more on the NADW production, which responds more dynamically in the 21st century to climate change and does not require high model resolution along the coasts. It is important to improve the representation of AABW in our state of the art ESMs, particularly as the focus shifts from year 2100 projections to the longer timescales more relevant for studying ocean-climate interactions.

It is important to note that at the end of the simulation in year 2300 the ocean was in the midst of a massive climate-driven transition in the physical and biogeochemical state, and was not close at all to achieving a new steady state. The oceans were still warming rapidly, modifying circulation and density structure. The depletion of upper nutrients and transfer to the deep ocean was ongoing, in a linear, continuing trend at year 2300, suggesting centuries more of biological productivity declines (MET2018). Thus, ESM simulations well past year 2300 are necessary to understand potential climate warming impacts on the oceans. The non-steady state complicates interpretation of the patterns of regenerated and preformed nutrients. Most previous studies examined this partitioning in the context of a steady state or even constant ocean circulation (i.e., Primeau et al., 2013; Pasquier and Holzer, 2016). In this context, increasing regenerated carbon in the deep ocean implies a more efficient biological pump and lower atmospheric CO_2 concentrations. Here deep ocean regenerated carbon and nutrients are increasing, even as the biological pump is becoming weaker over time, due to the circulation slowdown. In addition, the increasing storage of natural DIC in the deep ocean is having little impact on air-sea CO_2 exchange because the atmosphere has reached such high values and much of the surface ocean is saturated with CO_2.

The slowdown in the thermohaline circulation reduced the capacity for further uptake of heat and anthropogenic CO_2 by the oceans. Once low-latitude surface waters become saturated with anthropogenic CO_2 the main control on ocean uptake is how quickly the circulation brings up older, deeper waters with little or no anthropogenic CO_2, which have more uptake capacity. The Southern Ocean dominated CO_2 uptake by the 2290s, as older, deep waters still upwelling to the surface (MET2018). The slowing of the meridional overturning circulation, weakens the ocean capacity to take up anthropogenic CO_2, by reducing the exposure of undersaturated waters to the atmosphere and their subsequent return into the ocean interior. Similar arguments apply to the capacity for ocean heat uptake. By 2300 the oceans were still warming rapidly (Randerson et al., 2015), but the mean surface temperature at low latitudes (< 30 ^{o}Lat.) was leveling off after increasing by 6 ^{o}C, and the intermediate depth waters (~500-1500 m) were rapidly warming (MET2018). Thermodynamic feedbacks set an upper limit on surface warming in the tropics, effectively surface waters become thermally "saturated" with reduced capacity for additional warming. In a warming climate, the ocean heat uptake efficiency shows a tendency to reduce (Giorgetta et al., 2013). Mid-latitude surface water temperatures increased by up to 10 ^{o}C, and were still warming at 2300. The strongest ocean heat uptake occurs where cooler subsurface waters are brought to the surface by mixing

or upwelling. This phenomenon was increasingly restricted to the Southern Ocean in the CESM simulation, with increasing stratification suppressing vertical exchange elsewhere (MET2018).

The lack of active ice sheet dynamics affects our simulation in several ways. Ice-sheet interactions may impact AABW production rates as noted above. With the extreme climate warming simulated at high latitudes (surface air temperature warms by > 25 ^{o}C in some polar regions) the large ice sheets on Greenland and Antarctica would be releasing massive amounts of freshwater to polar surface waters, decreasing surface water density and intensifying the strong vertical salinity gradients already present. If the stratification increases enough in polar regions, there will be a complete shutdown of the overturning circulation, as surface waters can no longer attain the density necessary to sink into the deep ocean. If the stratification increases enough in the Southern Ocean it could break the last direct connection to the deep ocean at the Antarctic Divergence, by pulling in upwelling waters laterally from relatively shallow depths, rather than from the deep ocean. This is what occurs in the wind-driven upwelling zones at low latitudes today, where vertical density gradients are much stronger than in the Southern Ocean.

Such a complete break of the exchange between the surface and deep ocean would be catastrophic for the biosphere and the climate system. It would greatly accelerate the sequestration of nutrients in the deep ocean and the declines in deep ocean oxygen, driving even larger declines in global scale marine biological productivity and likely leading to widespread anoxia in the oceans. Severe hypoxia can lead to mass extinctions and even mild hypoxia can have strong effects on the physiology and activity levels of marine organisms (Doney et al., 2011; Stramma et al., 2010). The Permian mass extinction in the oceans was due to intensified stratification and widespread ocean anoxia, which may serve as an important ancient analog for future oceans (Payne and Clapham, 2012; Winguth and Winguth, 2012). Once such a mass extinction occurs, marine ecosystems need millions of years to recover the lost biodiversity and approach the original state (Song et al., 2011; Winguth and Winguth, 2012). It would also further extend the timescale for climate cooling by greatly reducing ocean uptake of heat and CO_2 from the atmosphere. Glacial flow also brings iron and other nutrients to the oceans fueling the biological production (Gerringa et al., 2012). Increased iron inputs in the Southern Ocean could intensify export production and the subsurface nutrient trapping, stripping even more of the nutrients out of the surface water transported to low latitudes, and further intensifying nutrient sequestration in the deep ocean. In addition, increased iron inputs may not reduce atmospheric CO_2 greatly due to the "leakage" effect (Oschlies et al., 2010).

5 Conclusions

Multicentury climate warming along the business as usual emissions trajectory induces Southern Ocean nutrient trapping, a greatly weakened global overturning circulation, increasing sequestration of nutrients and natural carbon in the deep ocean, and a reduced capacity for ocean uptake of heat and anthropogenic CO_2 from the atmosphere. This reduced uptake capacity could prolong, peak warmth, or hothouse Earth conditions for hundreds to thousands of years (Steffen et al., 2018). A global-scale weakening of the biological pump reduced oxygen demand in the deep ocean. However, the slowdown in the overturning circulation more than compensated for this by increasing deep-ocean water mean residence

time. This led to increasing nutrient concentrations and declining oxygen concentrations throughout the deep ocean. Inclusion of active ice sheet dynamics would further intensify stratification in polar surface waters, perhaps leading to a complete shutdown of the overturning circulation, extending the timescale for climate cooling by thousands of years and generating widespread ocean anoxia, which would drive a new mass extinction event.

Acknowledgements

We received support from the Reducing Uncertainty in Biogeochemical Interactions through Synthesis and Computation (RUBISCO) Scientific Focus Area (SFA) in the Regional and Global Climate Modeling Program in the Climate and Environmental Sciences Division of the Biological and Environmental Research Division of the US Department of Energy Office of Science (also DOE BER Earth System Modeling Program grant DE-SC0016539 to J.K.M. and F.P.). Additional support was provided by the National Science Foundation (grant 1658380). The Coupled Model Intercomparison Project received support from the World Climate Research Programme and the US Department of Energy's Program for Climate Model Diagnosis and Intercomparison. Computational and other support provided by the National Center for Atmospheric Research. The National Center for Atmospheric Research is sponsored by the National Science Foundation. All the data analyzed in this paper has been uploaded to zenodo with doi: 10.5281/zenodo.3596187.

References

Bopp, L., Resplandy, L., Orr, J. C., Doney, S. C., Dunne, J. P., Gehlen, M., Halloran, P., Heinze, C., Ilyina, T., Séférian, R., Tjiputra, J., and Vichi, M (2013).: Multiple stressors of ocean ecosystems in the 21st century: projections with CMIP5 models, Biogeosciences, 10, 6225–6245, doi:10.5194/bg-10-6225-2013.

Bronselaer, B., L. Zanna, D. R. Munday, and J. Lowe (2016), The influence of Southern Ocean winds on the North Atlantic carbon sink, Global Biogeochem. Cycles, 30, 844–858, doi:10.1002/2015GB005364.

Caesar, J., Palin, E., Liddicoat, S., Lowe, J., Burke, E., Pardaens, A., Sanderson, M., and R. Kahana (2013) Response of the HadGEM2 Earth System Model to Future Greenhouse Gas Emissions Pathways to the Year 2300. J. Climate, 26: 3275-3284.

Danabasoglu, G., Bates, S. C., Briegleb, B. P., Jayne, S. R., Jochum, M., Large, W. G., ... & Yeager, S. G. (2012). The CCSM4 ocean component. Journal of Climate, 25(5), 1361-1389.

Doney, S. C., Ruckelshaus, M., Duffy, J. E., Barry, J. P., Chan, F., English, C. A., ... & Polovina, J. (2011). Climate change impacts on marine ecosystems.

Dutkiewicz, S., M. Follows, and P. Parekh (2005), Interactions of the iron and phosphorus cycles : A three-dimensional model study, Global Biogeochem. Cycles, 19, doi :10.1029/2004GB002342.

Friedlingstein, P., Meinshausen, M., Arora, V. K., Jones, C. D., Anav, A., Liddicoat, S. K., & Knutti, R. (2014). Uncertainties in CMIP5 climate projections due to carbon cycle feedbacks. Journal of Climate, 27(2), 511-526.

Frölicher, T. L., Sarmiento, J. L., Paynter, D. J., Dunne, J. P., Krasting, J. P., & Winton, M. (2015). Dominance of the Southern Ocean in anthropogenic carbon and heat uptake in CMIP5 models. Journal of Climate, 28(2), 862-886.

Fu, W., Randerson, J. T., & Moore, J. K. (2016). Climate change impacts on net primary production (NPP) and export production (EP) regulated by increasing stratification and phytoplankton community structure in the CMIP5 models.

Fu, W., Primeau, F., J.K. Moore, J., Lindsay, K., & Randerson, J. T. (2018). Reversal of increasing tropical ocean hypoxia trends with sustained climate warming. Global Biogeochemical Cycles, 32, 551–564.

Gent, P. R., Danabasoglu, G., Donner, L. J., Holland, M. M., Hunke, E. C., Jayne, S. R., ... & Worley, P. H. (2011). The community climate system model version 4. Journal of Climate, 24(19), 4973-4991.

Gerringa, L.J.A., Alderkamp, A.C., Lann, P., Thuróczy, C.E., de Baar, H.J.W., Mills, M.M., van Dijken, G.L., van Haren, H., Arrigo, K.R., (2012) Iron from melting glaciers fuels the phytoplankton blooms in Amundsen Sea (Southern Ocean): Iron biogeochemistry. Deep-Sea Res. II, 71-76: 16-31. doi.org/10.1016/j.dsr2.2012.03.007.

Giorgetta, M. A., Jungclaus, J. H., Reick, C. H., Legutke, S., Brovkin, V., Crueger, T., Esch, M., Fieg, K., Glushak, K., Gayler, V., Haak, H., Hollweg, H.-D., Ilyina, T., Kinne, S., Kornblueh, L., Matei, D., Mauritsen, T., Mikolajewicz, U., Mueller, W. A., Notz, D., Raddatz, T., Rast, S., Redler, R., Roeckner, E., Schmidt, H., Schnur, R., Segschneider, J., Six, K., Stockhause, M., Wegner, J., Widmann, H., Wieners, K.-H., Claussen, M., Marotzke, J., and Stevens, B. (2013) Climate change from 1850 to 2100 in MPI-ESM simulations for the Coupled Model Intercomparison Project, 5, doi:10.1002/jame.20038.

Hauck, J., Völker, C., Wolf-Gladrow, D., Laufkötter, C., Vogt, M., Aumont, O., Bopp, L., Buiten- huis, E., Doney, S. C., Dunne, J., Gruber, N., Hashioka, T., John, J., Le Quéré, C., Lima, I. D.,Nakano, H., Seferian, R., and Totterdell, I.(2015), On the Southern Ocean CO2 uptake and the role of the biological carbon pump in the 21st century, Global Biogeochem. Cycles, 29, 1451–1470, doi:10.1002/2015GB005140.

Hofmann, M., & Schellnhuber, H. J. (2009). Oceanic acidification affects marine carbon pump and triggers extended marine oxygen holes. Proceedings of the National Academy of Sciences, 106(9), 3017-3022.

Ito, T., A. Bracco, C. Deutsch, H. Frenzel, M. Long, and Y. Takano (2015), Sustained growth of the Southern Ocean carbon storage in a warming climate. Geophys. Res. Lett., 42, 4516–4522. doi: 10.1002/2015GL064320.

Keeling, R. F., Koertzinger, A. & Gruber, N. (2010), Ocean deoxygenation in a warming world. Annual Review of Marine Science 2, 199-229, doi:10.1146/annurev.marine.010908.163855.

555 Leung, S., Cabré, A., & Marinov, I. (2015). A latitudinally banded phytoplankton response to
556 21st century climate change in the Southern Ocean across the CMIP5 model
557 suite. Biogeosciences, 12(19), 5715-5734.
558
559 Lindsay, K., G. B. Bonan, S. C. Doney, F. M. Hoffman, D. M. Lawrence, M. C. Long, N.
560 Mahowald, J. K. Moore, J. T. Randerson, and P. E. Thornton (2014), Preindustrial control
561 and 20th century carbon cycle experiments with the Earth system model CESM1(BGC), J.
562 Clim., doi:10.1175/ JCLI-D-12-00565.1.
563
564 Long, M. C., K. Lindsay, S. Peacock, J. K. Moore, and S. C. Doney (2013), Twentieth-
565 century oceanic carbon uptake and storage in CESM1(BGC), J. Clim., 26(18), 6775–6800,
566 doi:10.1175/jcli-d-12-00184.1.
567
568 Marinov, I., Gnanadesikan, A., Sarmiento, J. L., Toggweiler, J. R., Follows, M., & Mignone,
569 B. K. (2008). Impact of oceanic circulation on biological carbon storage in the ocean and
570 atmospheric pCO2. Global Biogeochemical Cycles, 22(3).
571
572 Marinov, I., A. Gnanadesikan, J. R. Toggweiler, and J. L. Sarmiento (2006), The
573 Southern Ocean biogeochemical divide, Nature, 441, 964–967, doi :10.1038/nature04883.
574
575 Moore, J. K., Lindsay, K., Doney, S. C., Long, M. C., & Misumi, K. (2013). Marine
576 ecosystem dynamics and biogeochemical cycling in the Community Earth System Model
577 [CESM1 (BGC)]: Comparison of the 1990s with the 2090s under the RCP4. 5 and RCP8. 5
578 scenarios. Journal of Climate, 26(23), 9291-9312.
579
580 Moore, J. K., S. C. Doney, and K. Lindsay, (2004), Upper ocean ecosystem dynamics and
581 iron cycling in a global three-dimensional model, Global Biogeochem. Cycles, 18, GB4028,
582 doi:10.1029/2004GB002220.
583
584 Moore, J. K., Fu, W., Primeau, F., Britten, G. L., Lindsay, K., Long, M., et al., (2018),
585 Sustained climate warming drives declining marine biological productivity, Science,
586 359(6380), 1139–1143.
587
588 Orsi, A. H., Johnson, G. C., & Bullister, J. L. (1999). Circulation, mixing, and production of
589 Antarctic Bottom Water. Progress in Oceanography, 43(1), 55-109.
590
591 Orsi, A. H., Smethie Jr, W. M., & Bullister, J. L. (2002). On the total input of Antarctic
592 waters to the deep ocean: A preliminary estimate from chlorofluorocarbon
593 measurements. Journal of Geophysical Research: Oceans, 107(C8), 31-1.
594
595 Oschlies, A., W. Koeve, W. Rickels, and K. Rehdanz (2010), Side effects and accounting
596 aspects of hypothetical large-scale Southern Ocean iron fertilization, Biogeosciences, 7,
597 4017–4035, doi :10.5194/bg-7–4017-2010.
598
599 Pasquier, B., and M. Holzer (2016), The plumbing of the global biological pump: Efficiency
600 control through leaks, pathways, and time scales, J. Geophys. Res. Oceans, 121, 6367–6388,
601 doi:10.1002/2016JC011821.
602

603 Payne, J. L., & Clapham, M. E. (2012). End-Permian mass extinction in the oceans: an
604 ancient analog for the twenty-first century?. Annual Review of Earth and Planetary
605 Sciences, 40, 89-111.
606
607 Primeau, F. W., M. Holzer, and T. DeVries (2013), Southern Ocean nutrient trapping and the
608 efficiency of the biological pump, J. Geophys. Res. Oceans, 118, 2547–2564,
609 doi :10.1002/jgrc.20181.
610
611 Randerson, J. T., Lindsay, K., Munoz, E., Fu, W., Moore, J. K., Hoffman, F. M., Mahowald,
612 N. M., and Doney, S. C. (2015) Multicentury changes in ocean and land contributions to the
613 climate-carbon feedback, Global Biogeochem. Cycles, 29, 744–759,
614 doi:10.1002/2014gb005079.
615
616 Sarmiento, J. L., N. Gruber, M. A. Brzezinski, and J. P. Dunne (2004), High-latitude controls
617 of thermocline nutrients and low latitude biological productivity, Nature, 427, 56–60.
618
619 Song, H., Wignall, P. B., Chen, Z. Q., Tong, J., Bond, D. P., Lai, X., ... & Chen, J. (2011).
620 Recovery tempo and pattern of marine ecosystems after the end-Permian mass
621 extinction. Geology, 39(8), 739-742.
622
623 Steffen, W., Rockström, J., Richardson, K., Lenton, T. M., Folke, C., Liverman, D., ... &
624 Donges, J. F. (2018). Trajectories of the Earth System in the Anthropocene. Proceedings of
625 the National Academy of Sciences, 115(33), 8252-8259.
626
627 Steinacher, M., Joos, F., Frölicher, T. L., Bopp, L., Cadule, P., Cocco, V., Doney, S. C.,
628 Gehlen, M., Lindsay, J.K., Moore, J. K., Schneider, B., and Segschneider, J., (2010),
629 Projected 21st century decrease in marine productivity: a multi-model analysis,
630 Biogeosciences, 7, 979-1005.
631
632 Stramma, L., Johnson, G. C., Sprintall, J., & Mohrholz, V. (2008). Expanding oxygen-
633 minimum zones in the tropical oceans. science, 320(5876), 655-658.
634
635 Stramma, Schmidtko, S., Levin, L. A. & Johnson, G. C. (2010), Ocean oxygen minima
636 expansions and their biological impacts. Deep Sea Research Part I: Oceanographic Research
637 Papers 57, 587-595, doi:10.1016/j.dsr.2010.01.005.
638
639 Van Vuuren, D. P., Edmonds, J., Kainuma, M., Riahi, K., Thomson, A., Hibbard, K., ... &
640 Masui, T. (2011). The representative concentration pathways: an overview. Climatic
641 change, 109(1-2), 5.
642
643 Winguth, C., & Winguth, A. M. (2012). Simulating Permian–Triassic oceanic anoxia
644 distribution: Implications for species extinction and recovery. Geology, 40(2), 127-130.
645

Figures

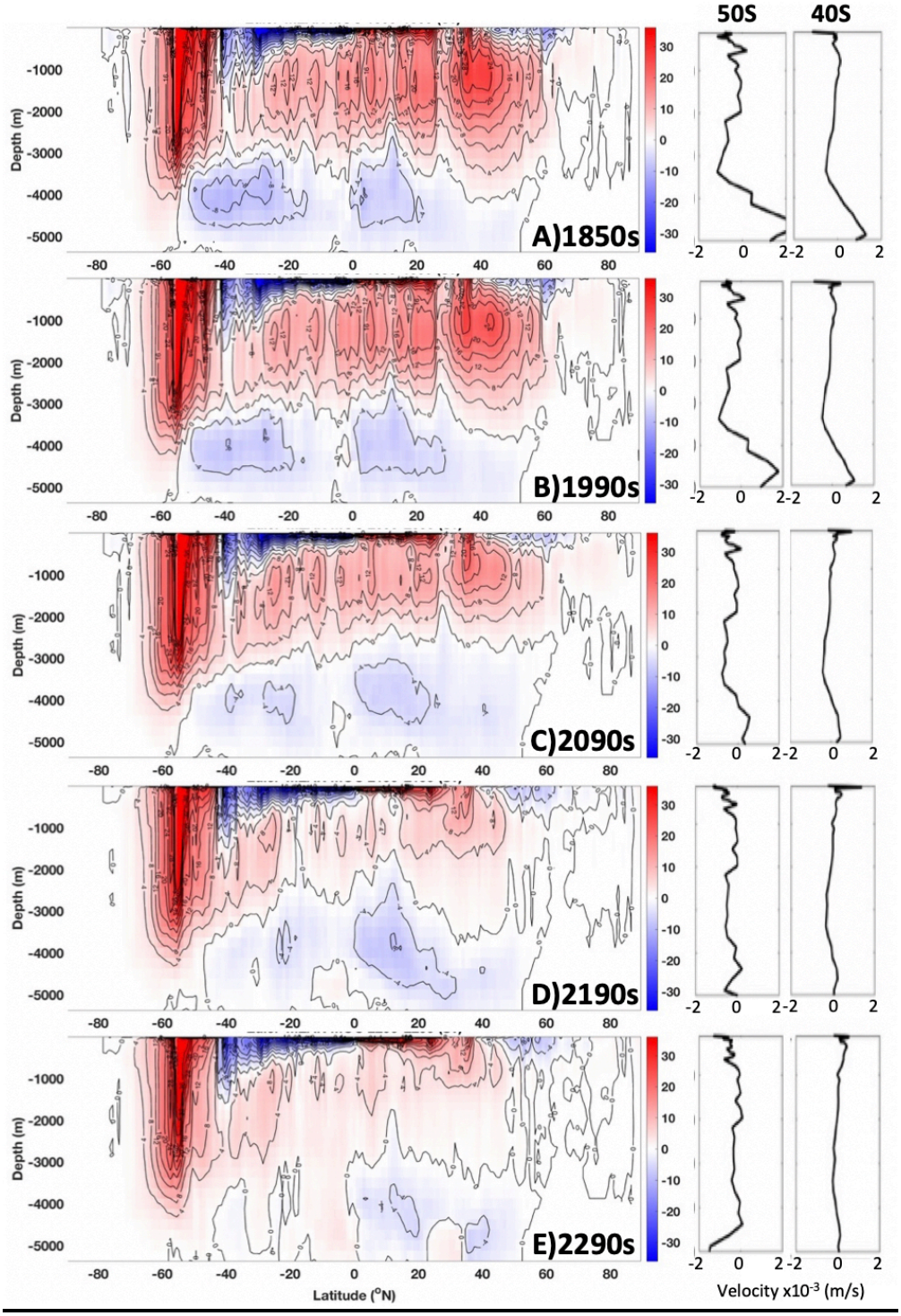

Figure 1. Global mean meridional stream function (Sv) and mean meridional velocity (m/s) across 40 ºS and 50 ºS are shown for key decadal periods.

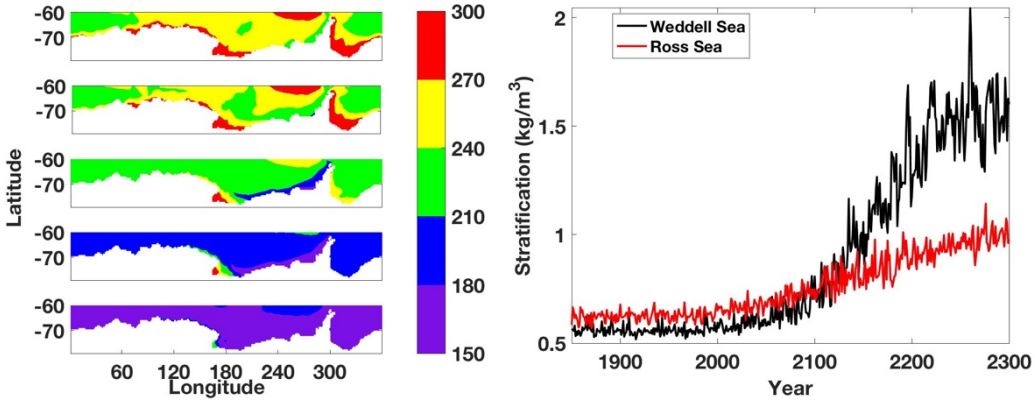

Figure 2. The dissolved oxygen (DO) distribution (mmol/m^3) at the shelf depth (200-400m) of Weddell Sea and Ross Sea in 1850s, 1990s, 2090s, 2190s and 2290s from top to bottom (a), time series of stratification (kg/m^3, calculated by $\rho_{200m} - \rho_{0m}$) in the Weddell Sea (black line) and Ross Sea (red line), respectively (b).

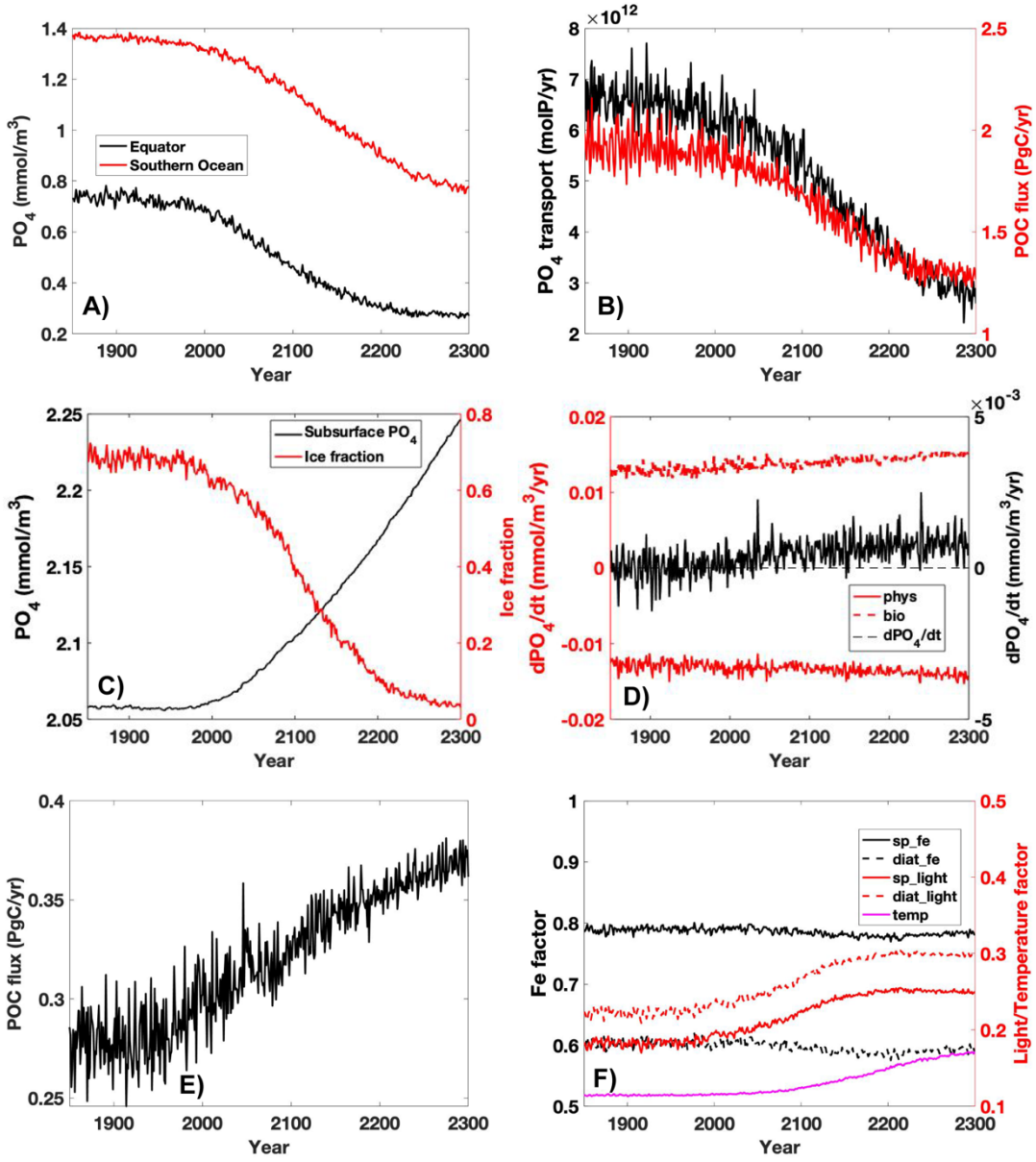

Figure 3. Surface PO_4 concentration at 50°S (in red) and in the equatorial region (in black, 10°S-10°N), are shown in panel A. Northward Ekman transport of phosphate across 50°S (in black) and integrated POC export in the equatorial region (in red) are shown in panel B. Time series of subsurface PO_4 and sea ice fractional cover (a), dPO_4/dt, with the physical contributions (i.e. advection and diffusion term) and biological contributions in the subsurface layer (100-1000m) (b), POC flux at 100m (c) and annual mean Fe and light limitation terms for small phytoplankton and diatom averaged over the mixed layer (d).

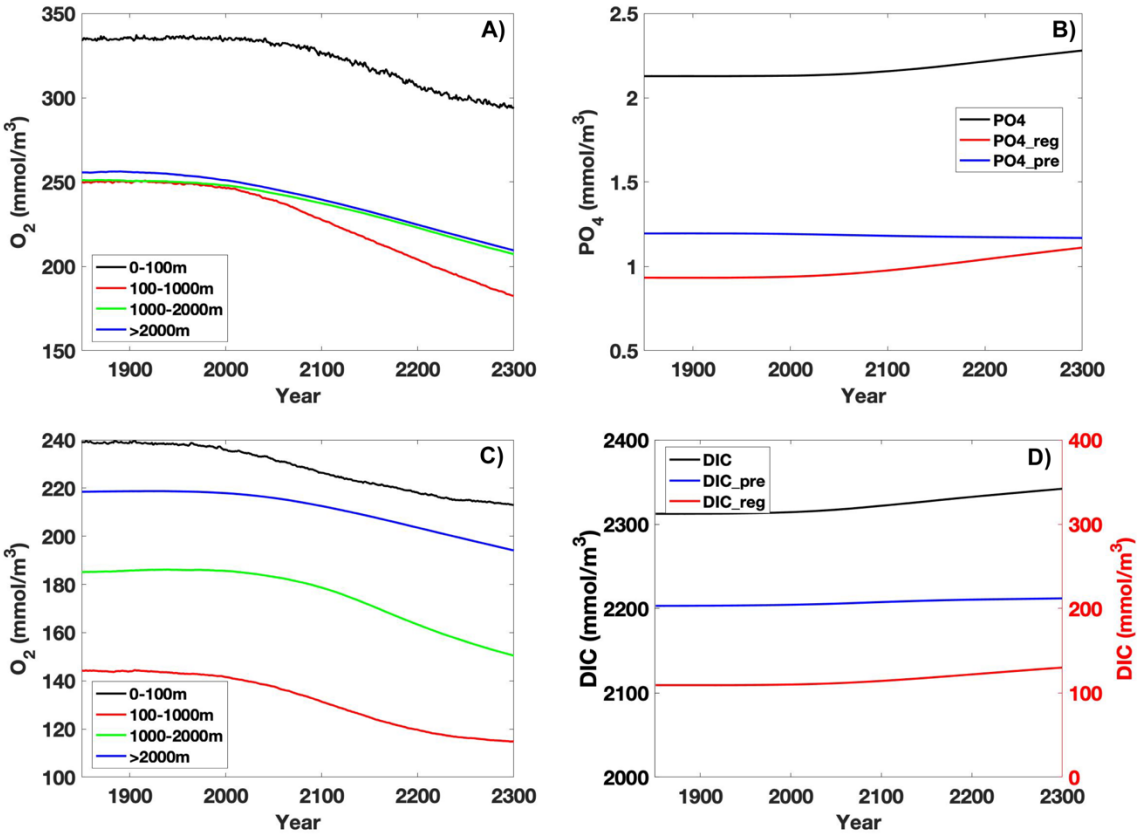

Figure 4. Time series of dissolved oxygen concentrations in the Southern Ocean (A) (90°S-60°S) and for the global ocean (C). Time series of total phosphate (black line), regenerated phosphate (red line) and preformed phosphate (blue line) in the deep ocean (> 2000 m) are shown in panel B, and total, regenerated and preformed DIC in the deep ocean are shown in panel D.

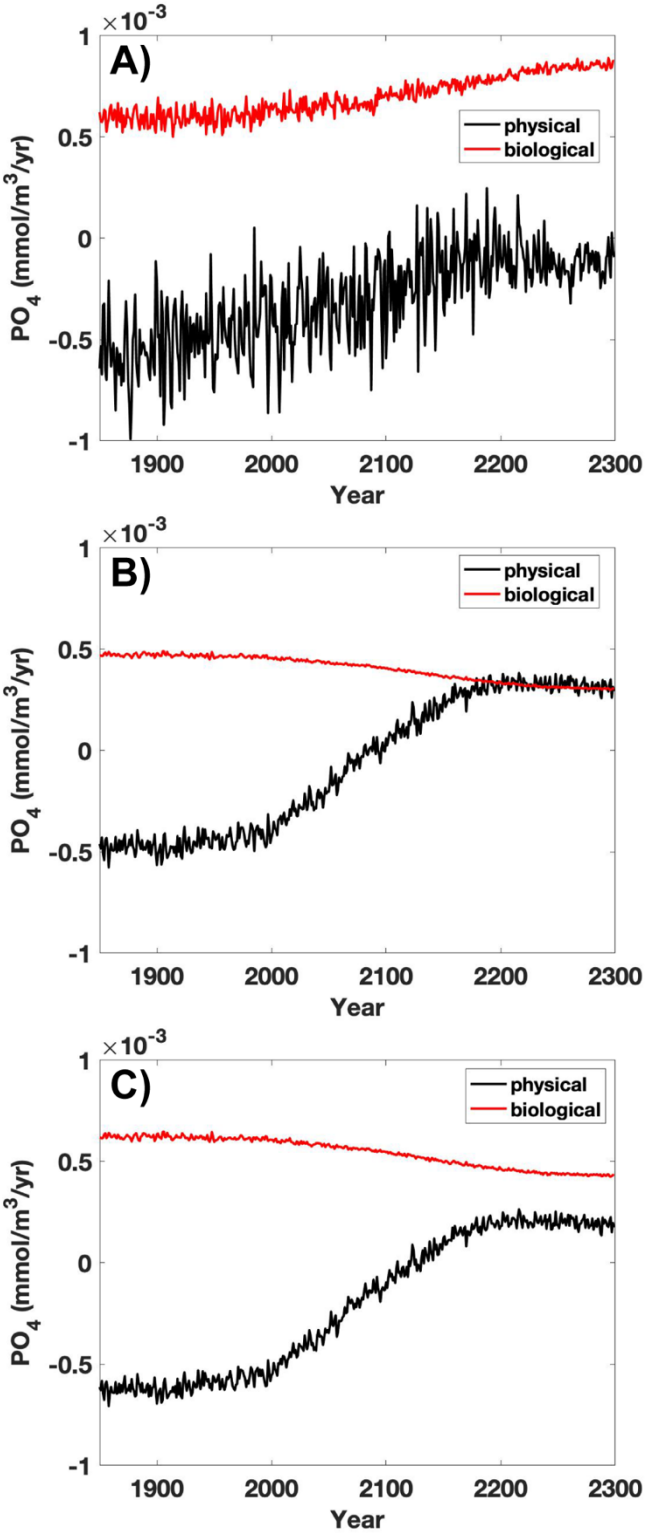

Figure 5. Physical and biological contributions to the deep-ocean (> 2000m) temporal change in phosphate concentration for (a) the Southern Ocean (90°S-60°S), (b) the rest of the oceans (60°S-90°N), and (c) the global ocean (90°S-90°N).

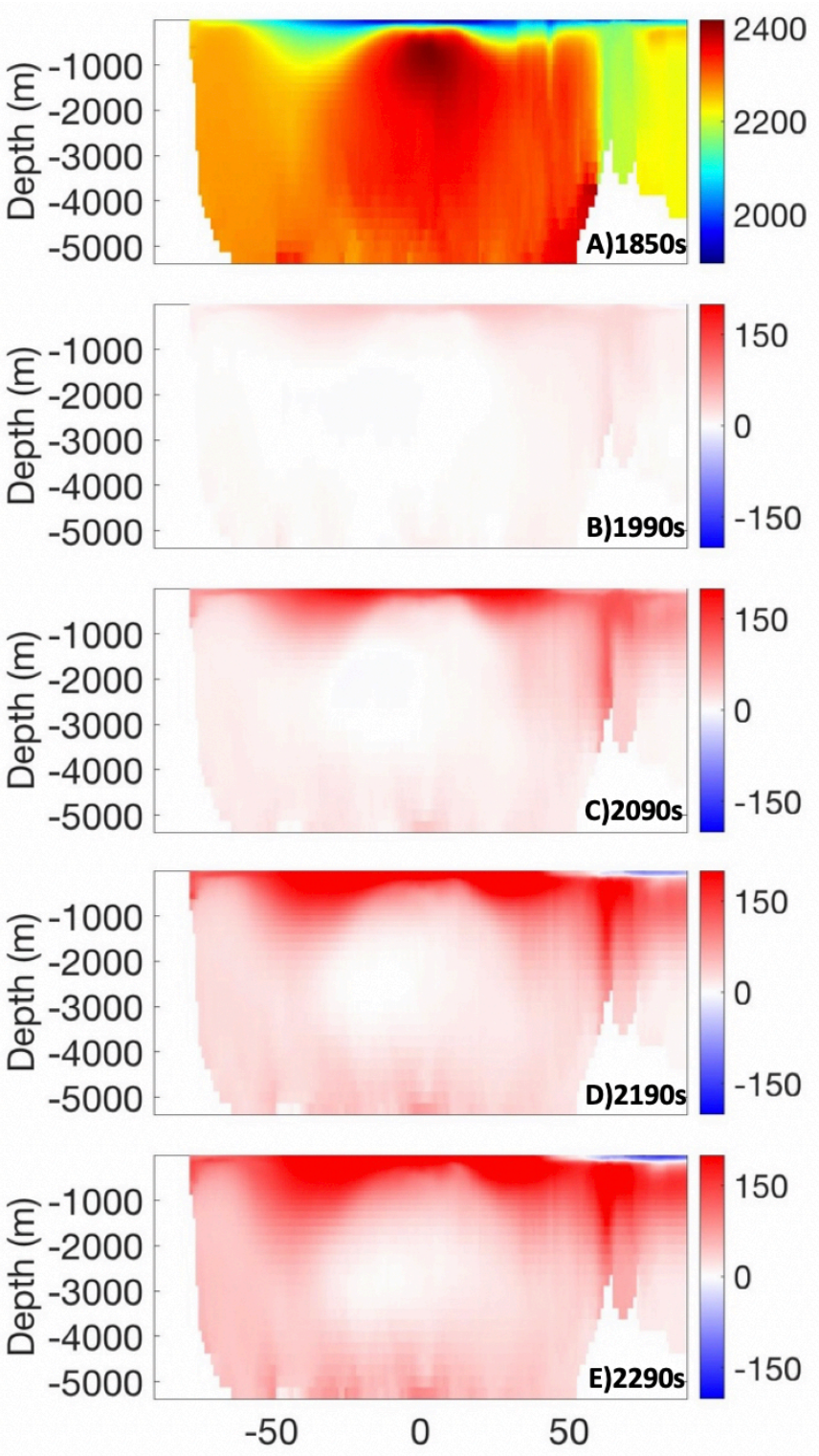

Figure 6. Global distribution of DIC in (A) 1850s, and difference plots for (B) 1990s-1850s, (C) 2090s-1850s, (D) 2190-1850s and (E) 2290s-1850s (mmol/m^3).